DESIGN OPTIMIZATION OF ACTIVE TWIST ROTOR BLADES

Carlos E. S. Cesnik† Jiwon Mok Jorge A. Morillo Anish S. Parikh

Department of Aerospace Engineering
The University of Michigan
Ann Arbor, MI 48109, U.S.A.

Abstract

This paper presents an optimization framework for designing active twist helicopter rotor blade cross-sections with embedded anisotropic piezocomposite actuators. On this work, the developed framework is applied to design a cross-section layout that maximizes the static twist actuation while satisfying a series of blade requirements. These requirements are associated with locations of center of gravity and elastic axis, blade mass per unit span, rotating blade frequencies, and blade strength based on local three-dimensional stress and strain fields under worst loading conditions. An active composite cross-sectional analysis (UM/VABS) and a geometrically exact one-dimensional beam analysis (DYMORE) along with other related analysis routines, including a cross-sectional parametric mesh generator, are combined with a gradient-based optimizer within MATLAB. The developed optimization framework is exemplified by using the NASA/Army/MIT Active Twist Rotor Blade and its baseline design. By using this methodology, a study is conducted to determine how some of the variables involved in the design influence the blade cross-sectional properties to maximize the static twist actuation.

Introduction

High vibration loads during forward flight conditions have been one of the major operation concerns that rotorcraft designers have been trying to solve during the last two decades. To alleviate this high vibration levels, integral twist actuation has been proposed and proved to have several potential benefits over the other active methodologies. By individually controlling each blade twist, local changes to the vibratory loads will result. If this is done at the appropriate phase, it will result in a reduction of the vibrations transmitted to the fuselage through the rotor hub.

In the NASA/Army/MIT Active Twist Rotor program, analysis and design methodologies were developed for active blades with embedded piezocomposite actuators (Ref 1). Using these methodologies, an ATR prototype blade was designed and fabricated for bench/hover tests (Ref 2). After minor design modifications, a set of active blades was manufactured and wind-tunnel tested in forward flight (Ref 3). During the open-loop forward flight test, significant authority on both fixed-and rotating-system loads was observed from the twist actuation. Finally, a closed-loop controller was designed to reduce the ATR hub vertical shear vibratory loads and implemented successfully in the Langley wind tunnel experimental testbed (Ref 4).

The blade design for that program was accomplished through exploration of several design candidates based on an existing passive blade (Ref 5). Through different candidates, several design variables were varied, such as the number of active layers, length of the active region in the chordwise direction, and the location of the active layers inserted in the cross section. Among those candidates, the one that exhibited the largest static twist actuation performance was selected as the final design candidate (Ref 5). Simultaneously, the other blade design parameters were kept at an appropriate range to give similar characteristics as the ones from the baseline passive blade. Although a feasible final design was obtained through the procedure described above, it was a time-consuming process with limited applicability. Different studies have been conducted that show numerical and experimental evidence that varying the distribution of passive and active materials in the cross section can improved the blade twist actuation authority (Ref 6 and 7). Nevertheless, even though important conclusions were presented, the manually-driven iterative process did not guarantee an optimum design at the end. The development of optimum design of active twist blades is a complex task, involving a rich design space with tightly coupled design variables. It is a problem ideally addressed using the principles of mathematical optimization that combine all the design variables and obtain the best design solution within the given constraints.

There have been different studies in the literature that apply the principle of mathematical optimization

† Corresponding author. 1320 Beal Avenue—3024 FXB, Ann Arbor, MI, 48109-2140, USA. E-mail: cesnik@umich.edu.

into the design of rotor blades, examples of which can be found in Refs. 8, 9, and 10. These studies focused on the design optimization of passive rotor blades, particularly to minimize vibration. When dealing with active blade design, another layer of complexity is added to the problem. An indirect way of addressing vibration control is by maximizing actuator authority. This must happen while a series of other constraints are being satisfied.

In this paper, a sensitive study to some of the design variables is conducted by using the developed optimization design framework for active helicopter blades with embedded piezocomposite actuators.

Optimization Design Framework

As introduced in the previous section, the proposed framework should seek for the optimum cross-sectional design of an active twist rotor blade with embedded piezocomposite actuators. In mathematical terms, the problem can be stated as:

$$max\ f(x) \tag{1}$$

subject to:

$$g(x) \le 0 \tag{2}$$

$$x_l \le x \le x_u \tag{3}$$

where f represents the static tip twist induced in the blade by the embedded piezocomposite actuators, x is the set of design variables that are bound between a lower (x_l) and an upper (x_u) limits, and $g(x)$ represents the set of nonlinear constraints.

As illustrated in Fig. 1, the design variables that can be used in the optimization problem are:

(a) The thickness and lamination angle of each ply in the cross-section lay-up. The material properties used in each ply, however, must be chosen in advance;
(b) The starting and ending locations of the active region;
(c) The chordwise location of the spar (web) wall;
(d) The length of the web extension;
(e) Two discrete ballast weights with their masses and chordwise locations.

These variables may be introduced at different blade radius, and they may be linked within a given spanwise region or among different regions of the blade. In the current implementation, the blade planform is subdivided in four regions of predetermined length. Each region may have a different airfoil. The cross section of each of the first three most inboard regions will contain design variables in the proposed framework. The most outboard region represents the blade tip, and its cross-sectional layup may be linked with the one from the neighboring inboard region. The blade planform includes pretwist and tip droop/sweep, so to model modern helicopter blade configurations. Due to manufacturing constraints, the chordwise location of the spar web should be considered a single design variable along the blade radius. In fact, if more parameters need to be linked from practical manufacturing considerations, it can be done as well. Finally, the permissible range of each design variable type is also imposed based on practical considerations.

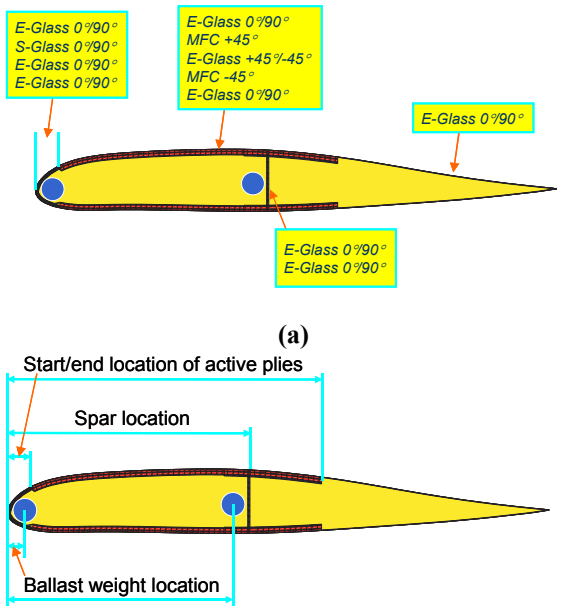

Figure 1: Illustration of (a) initial lay-up configuration for an ATR blade and (b) some of its design variables

Regarding the constraints ($g(x)$), the following set has been implemented in the proposed framework:

(a) Chordwise location of the cross-sectional center of gravity;
(b) Chordwise location of the cross-sectional elastic axis;
(c) Blade mass per unit span (for correct Lock number);
(d) Blade fundamental rotating frequencies (for desirable blade dynamics);
(e) Maximum allowable blade local strain under the worst-case loading condition (associated with the ultimate strength of the constituent materials).

Besides these, some extra constraints were added to better pose the problem (*e.g.*, end of the active region within the cross section must come at a chordwise location greater than the beginning of the same region, etc.). The implementation of the proposed framework is schematically described in Fig. 2. The environment used to integrate different analysis tools is MATLAB (Ref 11). In the implementation described in this paper, the following numerical tools are used:

UM/VABS, cross-sectional parametric mesh generator, DYMORE, 3-D strain module, and MATLAB.

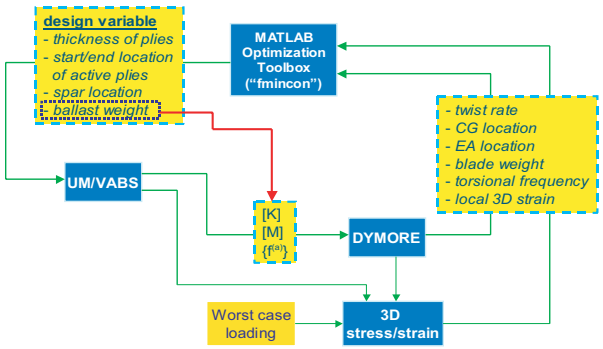

Figure 2: Flow chart of the design optimization framework for active twist rotor blades

UM/VABS is a finite-element based analysis of active cross sections with arbitrary geometry and material distributions (Ref 12). It provides cross-sectional stiffness, inertia and actuation forces/moments values to be used in the one-dimensional (beam) modeling of the blade. It also calculates the locations of the center of gravity and elastic axis, the blade mass per unit span, and the static active twist rate (in a given cross section). UM/VABS input has a NASTRAN-based format.

Since UM/VABS is a finite-element solver, it is crucial to have an automated mesh generator that can take a few parametric inputs and generate the needed mesh. This is accomplished with a MATLAB-based mesh generator specially developed for UM/VABS. To create a general airfoil wet surface, pairs of coordinate points defining the contour of the airfoil must be supplied. Contour equations have been implemented for the NACA four- and five-digit series airfoils. From the wet surface in, layers of given (composite) material are defined so to create the stacking sequence needed for the internal structural configuration. Materials are defined as both passive and active ones. Through a look-up table, their properties are loaded for each layer. Although UM/VABS can deal with any type of internal cross-sectional geometry, the mesh generator is limited to modeling walls and webs only (no foam or honeycomb filling, for example). The inertial effects associated with the ballast masses are added directly to the inertia matrix generated in UM/VABS.

Another important component part of the design framework is the one-dimensional global blade analysis. The analysis is conducted in DYMORE, a multibody dynamics code developed by Bauchau and co-workers (Ref 13). The exact solution of the geometric nonlinear beam problem provides the blade natural frequencies at normal rotating conditions. For the spanwise blade stations that correspond to a constant airfoil section, the cross-sectional analysis results obtained from UM/VABS are passed directly into DYMORE. At the short transitional stations between those blade regions, cross-sectional properties are assumed to be linearly varying with blade radius.

For given blade structural properties and loads, internal local 3-D strain and stress fields can be computed. In the current implementation, worst case sectional blade loads associated with flap bending, chordwise bending, and torsion must be supplied. Centrifugal forces are calculated within DYMORE and added to the set of those given loads. Although this may be at best a conservative estimate, it simplifies tremendously the design process. These loads can be evaluated off line with DYMORE or another aeroelastic code for a baseline blade configuration. They are then used with the information provided by UM/VABS to recover the local strain components at every cross-section point everywhere in the blade. The maximum strain criterion is applied for each of the components of the strain and compared to the allowable of the local constituent material. In the future, the prescribed loads will be replaced by an appropriate aeroelastic calculation for the exact structural properties within a given design cycle.

Finally, gradient-based constrained optimization is performed within MATLAB, using "fmincon" from its optimization toolbox. The "fmincon" function minimizes a constrained nonlinear multivariable problem. The medium scale option is used, which is associated with a sequential quadratic programming method. In each iteration, the function solves a quadratic programming subproblem (Ref 14), which improves convergence (Ref 15). The gradients of the objective function and the constraints are provided from finite difference (implemented in the framework). The BFGS (Broyden-Fletcher-Goldfarb-Shanno) method (Ref 16), a well-known quasi-Newton algorithm for unconstrained optimization, is used in this method. Three kinds of termination criteria have been applied: maximum number of iterations, tolerance on the design variables, and tolerance on the function value. When one of these termination criteria is satisfied, the optimization loop will end. In case the result indicates that the solution still needs more iterations, the optimization can be restarted from the point where it stopped previously.

Since the objective function is highly nonlinear, and since the design hyperspace is very complex, it is possible for "fmincon" to fall into a local extrema, leading to a sub-optimal solution. Therefore, it is necessary to run the optimization to completion, starting from different initial points. When the problem is infeasible, "fmincon" attempts to reduce the distance to the most violated constraint boundary. Thus, it is recommended to start with a feasible initial point if possible.

Numerical Examples

In order to exemplify the capabilities of the developed formulation, the NASA/Army/MIT ATR blade is used as a reference case. By selecting different sets of design variables and constraints, alternatives to the original design are generated.

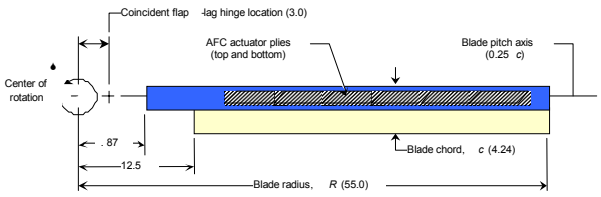

(a)

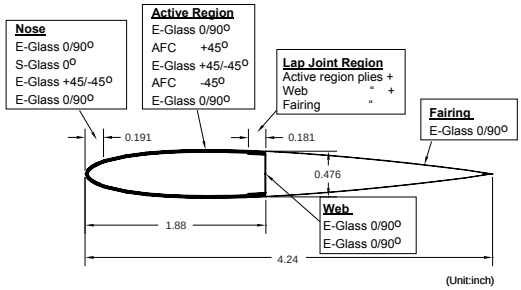

(b)

Figure 3: (a) Planform, and (b) cross section of the NASA/Army/MIT ATR blade (dimensions are in inches)

Table 1: Constraints and bounds for Case 1

Center of Gravity (CG)	0.2c < CG < 0.28c
Elastic Axis (EA)	0.17c < EA < 0.25c
Blade mass / length (kg/m)	0.656 < m < 0.72
1st torsional frequency (1T)	1T < 8/rev
Local Strain in the worst case loading	1.5xMax strain < ultimate strength of original constituent material
Ply thickness	0.5 < t_k < 5.0
Web extension	0.05c < web_{ext} < 0.1c
Active region	0.0455c< Loc<0.85c
Spar location	0.1c < $Spar_{loc}$ < 0.85c

Baseline ATR Blade Characteristics. As briefly described above, the original requirements for the NASA/Army/MIT ATR blade came from an existing passive blade used by NASA Langley. That blade has been well studied and characterized over the years, and it has the geometry and nondimensional characteristics that are representative of a generic production helicopter blade (Ref 5). The ATR blade was designed to be tested in heavy gas (R134a) medium. The design employed a total of 24 active fiber composite (AFC) actuators placed on the front D-spar only, and distributed in six stations along the blade span. The ATR final design was determined by manual iterations in search for maximum static twist actuation. Figure 3 shows ATR blade planform and its cross section. The airfoil is a NACA 0012. The material properties of the passive prepregs and the AFC plies used in the blade are summarized in the appendix of Ref 5. The original ATR design was successfully manufactured and tested and this will serve here as the reference for the optimization exercise.

Blade optimization with similar characteristics from ATR baseline case (Case 1). For this first case, the constraints are set such that the ATR reference blade design is a feasible solution, as summarized in Table 1. The objective is to determine the internal cross-section configuration such that the characteristics of the numerically optimized blade are the same as the ATR reference blade. Therefore, the problem resumes in maximizing the twist actuation while keeping airfoil, ply thicknesses and ply angles fixed. The design variables are only the length of the web extension, the spar location, ballast weights and their locations, and the start/end of the active regions. These give a total of 8 design variables, and their initial values are presented in Table 2 (corresponding to the ATR reference blade).

Table 2: Initial values of the design variables for Case 1

Active start	0.0455c
Active end	0.45c
Web extention	0.05c
Ballast weight mass	(0.23, 0.215)
Ballast Weight location	(0.027c, 0.432c)
Spar location	00.4438c

Table 3: Reference and optimization results for Case 1

	ATR reference blade	Case 1
Active layer properties	AFC	AFC
Tip twist	1	1.19
CG location (%c)	23.20	24.00
EA location (%c)	19.62	19.00
Blade mass/length (kg/m)	0.7103	0.70
1st torsional frequency (1/rev)	6.32	6.06
Strain in 1.5 worst case loading – shear (microstrain)	6327	6732

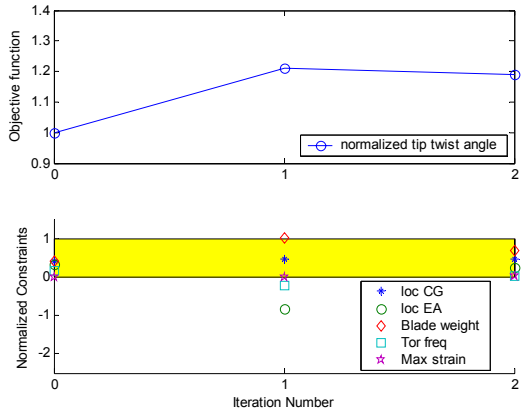

(a)

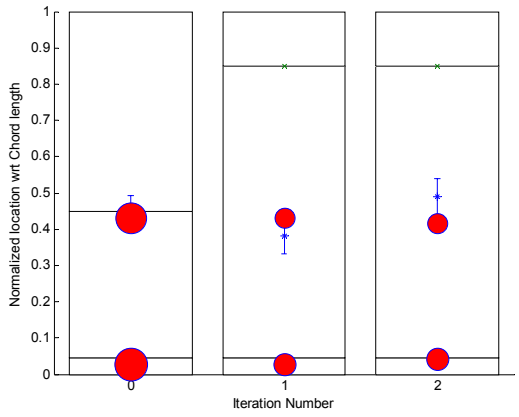

(b)

Figure 4: Case 1 results. (a) Objective function convergence history (top) and normalized blade parameters (bottom), and corresponding (b) spar location (*), web extension (|), front and rear ballast weights (•), and start and end of active region (- x -), all normalized by chord length

Table 4: Constraints for cases with improved characteristics from ATR baseline case

	Case 2(a)	Case 2(b), Case 3, and Case 4
Center of Gravity (CG)	0.2c < CG < 0.28c	
Elastic Axis (EA)	0.17c < EA < 0.25c	0.22c < EA < 0.28c
Blade mass / length (kg/m)	0.656 < *m* < 0.72	
1st torsional frequency (1T)	1T < 5/rev	
Local Strain in the worst case loading	1.5xMax strain < ultimate strength of original constituent material	
Spar location	0.1c < $Spar_{loc}$ < 0.85c	

Figure 4(a) shows the convergence history of the normalized (with respect to the ATR reference tip twist actuation) objective function and various normalized blade parameters: locations of the center of gravity and elastic axis, blade mass per unit length, first torsional frequency and the maximum strain. The shaded area represents the feasible range of these parameters. The convergence history of the spar location, length of the web extension, position of the front and rear ballast weights, and start and end of the active region are shown as function of the chordwise position in the airfoil in Fig. 4(b). As it can be seen, in only two iterations the maximum normalized tip twist reached 1.193. This indicates, for this particular case, an increase of approximately 20% over the ATR reference blade. The start and end chordwise location of the active region is pushed to the bounds. This indicates the desire of adding more active material in the cross section. The elastic axis location, 1st torsional frequency and the maximum strain were the active constraint in this case. The spar location was pushed back by approximately 5% to 0.49c and the elastic axis was located at 0.19c. The resulting length of the web extension was 5% chord. The front ballast mass was set aligned with the beginning of the active region, while the rear ballast mass ended up in front of the front web extension, near 0.418 chord placing the center of gravity at 0.238c. The 1st torsional frequency is 6.06/rev and the maximum strain (inplane shear strain) finishing right up against the allowable of 6800 microstrain. These results are summarized in Table 3 and compared with ATR reference blade (baseline).

Blade optimization to improve characteristics from ATR baseline case. Originally, it was desirable for the ATR blade to have both the center of gravity and the elastic axis located at 25% chord. This requirement comes from blade dynamics and aeroelastic stability considerations. Moreover, the blade first torsional frequency should be lower than 5.0/rev at the nominal rotating condition. However, these conditions were not achieved within the original ATR blade. Now, consider seeking for a new design solution that satisfies those constraints shown in Table 4 and providing at the same time a high twist actuation authority than the baseline case.

Three sub-cases are presented here:

(a) Case 2. This case uses the same set of design variables than Case 1, for a total of 8 variables, but subject to the constraints defined in Table 4. This case is used to analyze the effect that the constraint related with the location of the elastic axis has on the optimized design for the cross-section. Therefore, two different constraints for it are used. In Case 2(a) the elastic axis is forced to be located between the leading edge and the quarter cord

reference line, similarly constraint to Case 1. In Case 2(b), it is allowed to move a distance of 0.03c at both side of the quarter cord reference line.

(b) Case 3. Here the complete set of possible design variables are used, totaling 29 design variables. The "ply thickness" used here is actually the multiple of the nominal *prepreg* ply thickness. Although it should be an integer number, all design variables are treated as continuous ones.

(c) Case 4. Only the 12 ply angles constitute the set of design variables.

Tables 5 and 6 contain the initial values for the design variables.

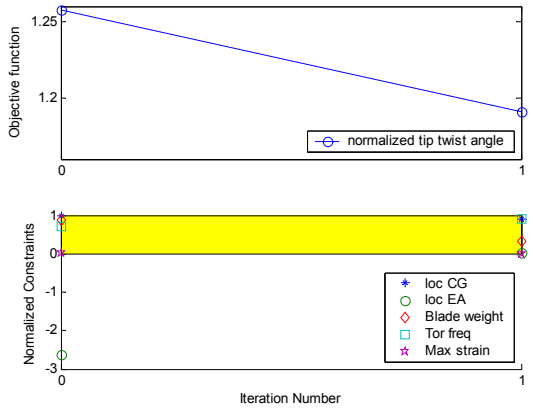

(a)

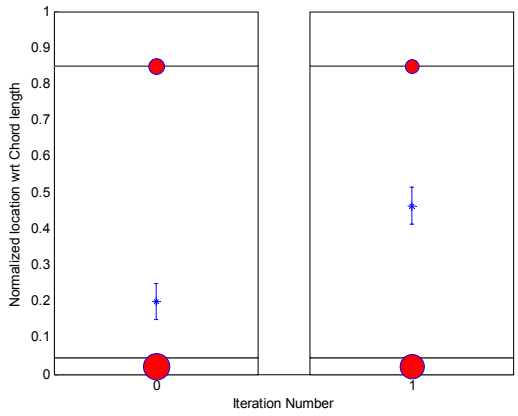

(b)

Figure 5: Case 2(a) results for initial spar location at 0.2c. (a) Objective function convergence history (top) and normalized blade parameters (bottom), and corresponding (b) spar location (*), web extension (|), front and rear ballast weights (•), and start and end of active region (- x -), all normalized by chord length

Table 5: Initial design values

	Case 2(a), (b)	Case 3
All ply thickness	1.0	1.0
Active start	0.0456c	0.0456c
Active end	0.85c	0.85c
Web extention	0.05c	0.05c
Ballast weight mass	(0.186, 0.105)	(0.186, 0.105)
Ballast Weight location	(0.022c, 0.85c)	(0.022c, 0.85c)
Spar location	0.2c, 0.634c	0.634c

Table 6: Initial design values

	Case 4
All ply thickness	1.0
Ply Angles (degrees)	[0 / 0 / +30 / -30 / +45 / -30 / +30 / 0 /0 / 0 / 0 / 0]
Active start	0.05c
Active end	0.85c
Web extension	0.05c
Ballast weight mass	(0.1765, 0.0863)
Ballast Weight location	(0.0c, 0.918c)
Spar location	0.609c

Table 7: Optimized values for Case 2(a)

I.C's for Spar location	0.2c	0.634c
Active start	0.0455c	
Active end	0.85c	
Web extension	0.05c	
Ballast masses (kg)	(0.175,0.095)	(0.169,0.096)
Ballast mass location	(0.02c, 0.85c)	
Spar location	0.465c	0.58c
Elastic Axis	0.17c	0.25c
Center of Gravity	0.28c	0.28c
Torsional Frequency	4.66	5.0
Normalized twist actuation	1.19	1.19
Strain in 1.5 worst case loading – shear (microstrain)	6773	6800

Figures 5(a) and 6(a) show the convergence history of the normalized objective function and various normalized blade parameters for Case 2(a) with two different initial values for the spar location, 0.2c and 0.634c, respectively. Similarly to Fig. 4, the shaded area represents the feasible range of these parameters. Notice that the only constraint that is not within the feasible range is the location of the elastic axis. The

convergence history of the spar location, length of the web extension, position of the front and rear ballast weights, and start and end of the active region are shown as function of the chordwise position in the airfoil in Figs. 5(b) and 6(b), and summarized in Table 7. Since the only active constraint violated is the elastic axis location, the spar location is the variable that acts to place it within the feasible range. For this case, the final location of the spar depends on the initial value given to this design variable. By given the spar location an initial value close to the lower bound, its final position is 0.465c, the elastic axis is located on its lower bound (0.17c), and the 1st torsional frequency is 4.66/rev. On the other hand, by using an initial value closer to the upper bound, the spar location converges to 0.58c, the elastic axis on its upper bound (0.25c), and the 1st torsional frequency to 5.0/rev. Similar twist actuation is obtained in both cases. This equivalence is associated with two competing effects. First, the optimizer wants to add active material in the frontal area of the airfoil section because that gives higher twist actuation per unit added active material than if the active material is added in the rear part of it (Ref. 7). For a given length of the active region, this can be achieved by moving the spar web aft. In the other hand, by moving the web to the front, effectively the optimizer is increasing the enclosed area of the rear part of the airfoil, therefore increasing the net induced active twist moment (Ref. 6). These two results are the limiting points of these two cases for maximum twist.

Figures 7 and 8 show the result for Case 2(b) with the same initial values for the spar location as Figs. 5 and 6, respectively. The optimized solution is summarized in Table 8. In this case, the spar location (0.635c), the location of the elastic axis (0.28c), torsional frequency (5.0 /rev), and normalized twist actuation (1.2) is not sensitive to the initial value of the spar location. The effect of letting the elastic axis moves to the right of the quarter cord reference line, allows the spar to move further back toward the trailing edge. When compare the optimized result for Case 2(a) with an initial spar location at 0.634c and any one solution for Case 2(b), it is observed that the elastic axis location and torsional frequency have the same values. Nevertheless, the twist actuation in Case 2(b) is slightly higher (1%) than in Case 2(a). As predicted in Ref 7, moving the spar further toward the trailing edge, increases the amount of active material placed on the front area of the cross-section, therefore an improvement in twist actuation is obtained.

Table 8: Optimized values for Case 2(b) for both initial conditions for spar location

Active start	0.0455c
Active end	0.85c
Web extension	0.05c
Ballast masses (kg)	0.163, 0.099
Ballast mass location	0.001c, 0.868c
Spar location	0.635c
Elastic Axis	0.28c
Center of Gravity	0.28c
Torsional Frequency	5.00
Normalized twist actuation	1.2
Strain in 1.5 worst case loading – shear (microstrain)	6800

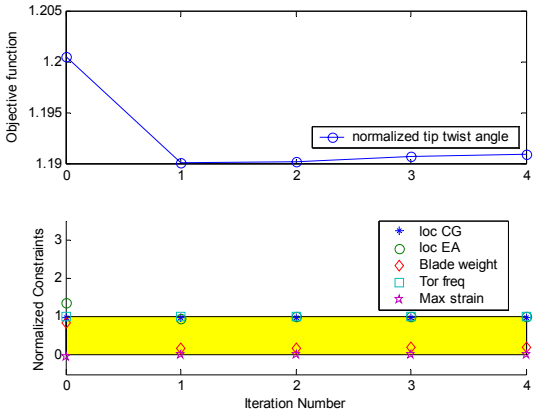

(a)

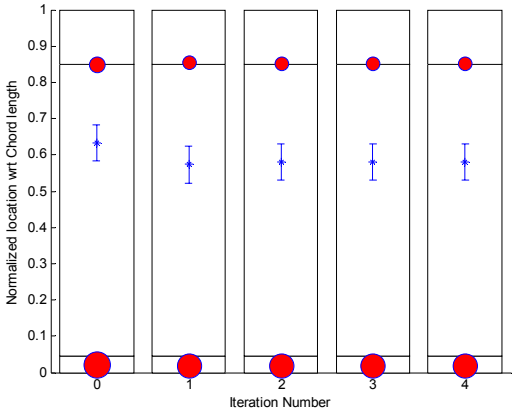

(b)

Figure 6: Case 2(a) results for initial spar location at 0.634c. (a) Objective function convergence history (top) and normalized blade parameters (bottom), and corresponding (b) spar location (*), web extension (|), front and rear ballast weights (•), and start and end of active region (- x -), all normalized by chord length

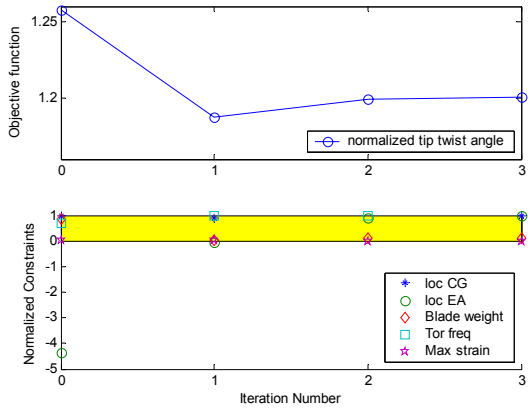

(a)

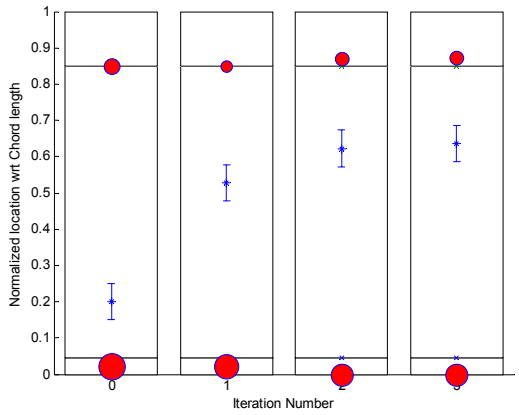

(b)

Figure 7: Case 2(b) results for initial spar location at 0.2c. (a) Objective function convergence history (top) and normalized blade parameters (bottom), and corresponding (b) spar location (*), web extension (|), front and rear ballast weights (•), and start and end of active region (- x -), all normalized by chord length

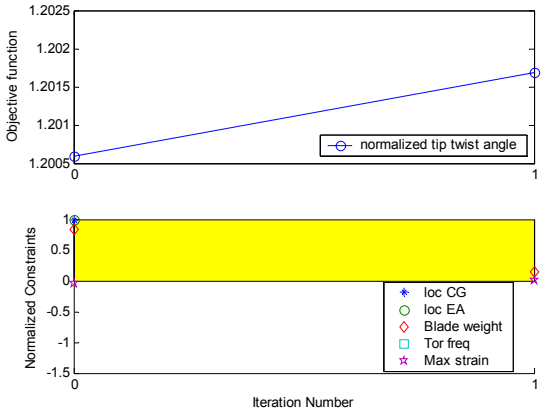

(a)

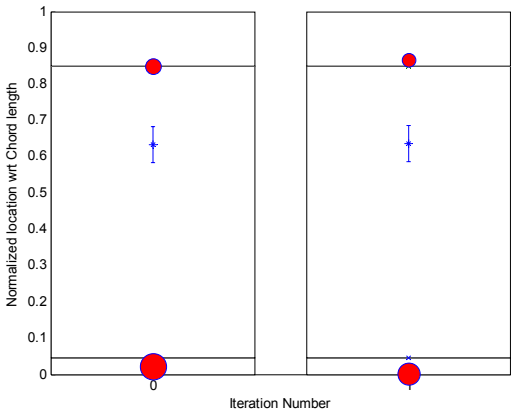

(b)

Figure 8: Case 2(b) results for initial spar location at 0.634c. (a) Objective function convergence history (top) and normalized blade parameters (bottom), and corresponding (b) spar location (*), web extension (|), front and rear ballast weights (•), and start and end of active region (- x -), all normalized by chord length

Figures 9 shows the convergence history of the normalized objective function and various normalized blade parameters for Case 3, as well as the convergence history of the spar location, length of the web extension, position of the front and rear ballast weights, and start and end of the active region as function of the chordwise position in the airfoil. Case 3 took 30 iterations to converge. The 1st torsional frequency was the most difficult variable to keep within the required bounds. The web location resulted at 0.747c, and the active region extends to its limits.

Figure 10(a) shows the evolution of the ply thicknesses with respect to the number of iterations. Results are between half de nominal ply thickness for the outer and web e-glass plies and 78% above the nominal ply thickness for the outer active composite ply. Since 0.5 is a lower bound for the thickness design variable, this indicates that the optimizer is trying to eliminate some of the plies in favor of others. Also, since the outer active plies have a bigger effect in twist than the inner ones, even thought both of these plies are increased over nominal thickness, the optimizer is allowing the outer ply to increase further than the inner one. The increment in nominal thickness is bound by the blade mass/length constraint which reaches its upper limit. The optimizer is following the behavior predicted in Ref 6 which indicates that by adding passive material on the nose region, an increment in

torsional stiffness is achieved, as well as an increase in twist actuation. On the other side, by adding passive material on the active material region results in a reduction in twist actuation.

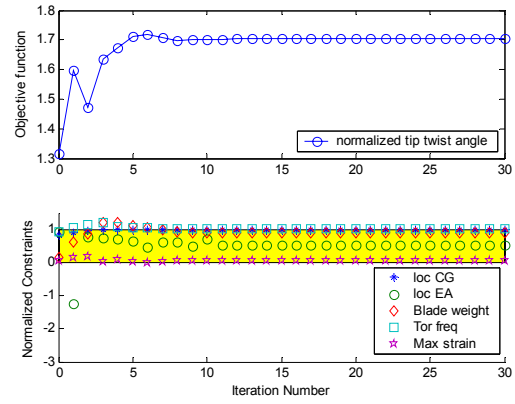

(a)

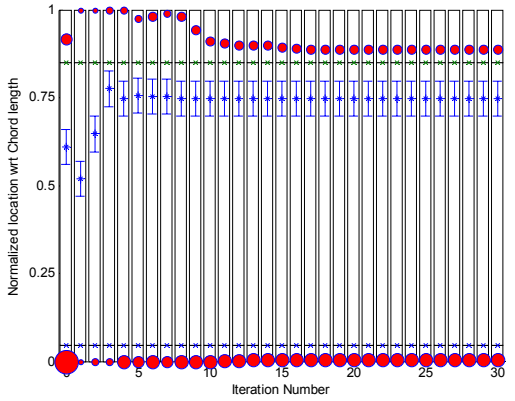

(b)

Figure 9: Case 3 results. (a) Objective function convergence history (top) and normalized blade parameters (bottom), and corresponding (b) spar location (*), web extension (|), front and rear ballast weights (•), and start and end of active region (- x -), all normalized by chord length

Figure 10(b) shows the ply angle variation during the optimization process. Even thought the set of design variables includes all the ply angles, Fig. 10(b) shows the active material plies, the passive between active materials, and nose plies. Ply angles for outer E-glass, web and web extension are not shown since they stay at 0°. Active ply angles converge to [+49°/-52°] instead of ±45° which are the ply angles for active material that would theoretically produce maximum twist actuation. Even thought further investigation on the convergence of the optimizer around this point is required, it is believe that the lack of sensitivity of the problem around the optimum point at ±45° for the active plies does not allowed the optimizer to reach that global minimum. It is worth noting that the ply angle for the nose moves up to –9° and the spar moves further back than Case 2(b), 0.747c. This decreases the stiffness and compensate for the material lost at the web, and help the elastic axis stays within the prescribed boundaries.

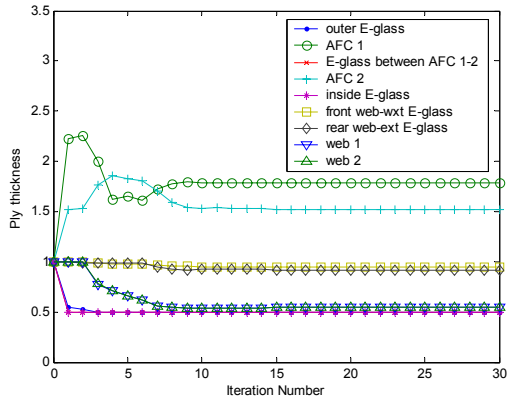

(a)

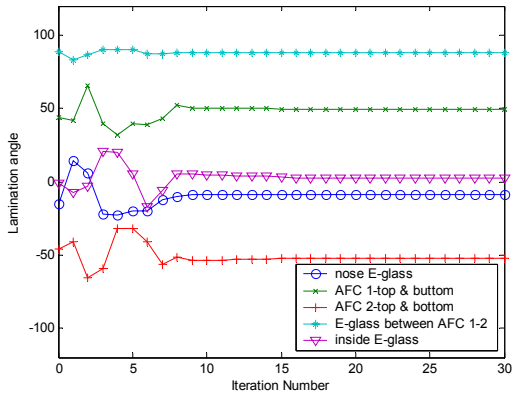

(b)

Figure 10: Evolution of (a) ply thickness and (b) ply angles for Case 3

Case 4 took 11 iterations to converge (Fig. 11(a)), and the normalized twist actuation obtained is 31% higher than the baseline case. Similar to Fig. 10(b), but now with the complete set of ply angles included among the design variables, Fig. 11(b) shows the convergence of ply angles for the active, the passive between active, and the nose plies. Again, it is observed that the ply angle from the active material ply converges to approximately ± 45°. Also, the nose E-glass ply angle moves slightly away from 0° toward –9°. These adjusted the torsional stiffness of the blade (final 1st torsional frequency is 4.89/rev) and the elastic axis location moved toward the leading edge to 0.252c. The final design does not present an active twist authority as high as the one from Case 3, but it is higher than Case 2.

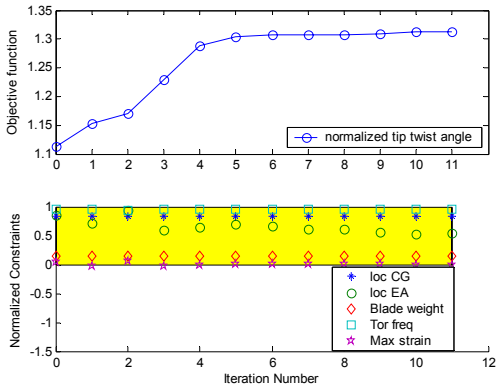

(a)

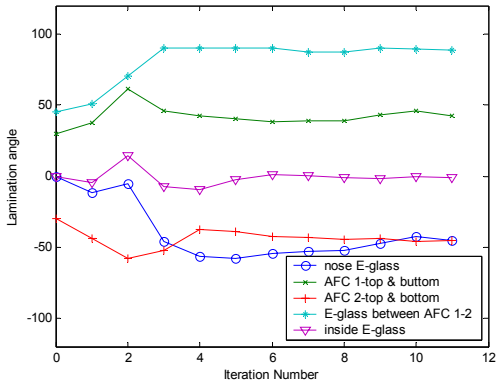

(b)

Figure 11: Case 4 results. (a) Objective function convergence history (top) and normalized blade parameters (bottom), and corresponding (b) Evolution of ply angles

Table 9: Optimized results for Cases 2, 3 and 4

	Case 2(a)	Case 3	Case 4
Tip twist (deg)	1.19	1.70	1.31
Spar location	0.58c	0.74c	0.60c
CG location (%c)	0.28c	0.28c	0.27c
EA location (%c)	0.25c	0.28c	0.25c
Blade mass/length (kg/m)	0.675	0.71	0.676
1st torsional frequency (1/rev)	4.66	5.0	4.83
Strain in 1.5 worst case loading – shear (microstrain)	6800	6628	6800

The results obtained by designing the cross-section by using the optimization framework are summarized in Table 9. From these results, the first thing to observe is that even though the constraints are tighter in these cases than they are in Case 1, a solution with better performance than the original ATR reference blade can still be obtained. In fact, Case 2 shows that the new constraints can be accommodated by the same set of design variables as in Case 1 and provides very similar twist actuation performance.

Among the three cases, Case 3 presents the highest twist actuation. However, since ply thicknesses are integer quantities (multiple of the nominal ply thickness), this optimum solution is not practical. Allowing an adjustment on the ply angles provided an extra 11% increase in the twist authority from Case 2.

General Observations and Recommendations

While running the optimization cases discussed previously, some practical observations can be made:

(a) The selection of the constraint for the elastic axis position has an important effect on the position of the spar along the cross-section. By allowing the elastic axis to be located between the quarter cord and the trailing edge, the spar will locate further back toward the trailing edge than if the elastic axis is forced to be between the leading edge and the quarter chord point.

(b) References 6 and 7 presented recommendations related to the most effective ways to add active and passive materials on the cross-section of an active twist rotor blade. By analyzing the numerical examples presented in this paper, it is observed that the proposed optimization framework presented trends in the variables that followed the observations made in those references.

(c) For the examples run, the maximum strain seemed to occur at the same place (or similar) every time: right at the point of discontinuity in ply thickness between the active region and the nose region in the cross section. Adding a passive ply in the nose seemed to reduce the stress concentration that arose from the discontinuity in ply thickness to the left of the active region (toward the leading edge). Additionally, by adding passive material in the nose, the actuation authority of the blade is increased.

(d) Even though all cases presented in this work correspond to symmetric airfoils (NACA 0012) the trends observed here are applicable to unsymmetric airfoils with similar thickness.

(e) It is very helpful to have three constraints associated with maximum strain (two normal and one inplane shear components) instead of just the single most critical component. This avoids discontinuity in the constraint, reducing its nonlinear characteristics. Also, by considering three components, the resulting strain/stress may be better distributed in the cross section.

(f) Including ply angles among the design variables made it more difficult for the optimizer to converge than the case in which the spar location, ballast

masses and location, web extension, and start and end position for the active material are used as design variables.

(g) The nonlinear nature of the problem under consideration and the chosen gradient-based optimization scheme, as expected, make the solution sensitive to the initial values of the design variables (local optimum). The optimizer converged much faster to a local optimum when the initial point was a feasible one.

Also, the following two points are recommended:

(a) The ability to eliminate an undesirable ply through reducing its thickness to zero should be implemented. For that, modifications must be made on the automated mesh generator.

(b) Implementing a mixed continuous/discrete optimization algorithm could be useful, especially for layer thicknesses and ply angles. Some preliminary work has started to investigate its feasibility for this problem.

Concluding Remarks

This paper presented an optimization framework for active helicopter rotor blade cross-sectional design. Within this, optimization studies were performed using the NASA/Army/MIT ATR blade case. The examples showed that the original ATR blade, successfully manufactured and tested, could exhibit at least 30% higher actuation performance if designed within the optimization framework proposed in this paper. This framework allows for the exploration of the rich and highly nonlinear design space facing the sizing of active twist rotor blades. Different analytical components are combined in the framework: cross-sectional analysis, automated mesh generator, one-dimensional beam solver, 3-D local strain module, and numerical optimization routine. Through the mathematical optimization problem, static twist actuation performance of a blade is maximized while satisfying certain blade constraints.

Acknowledgements

This work has been supported by NASA Langley Research Center under cooperative agreement NCC1-323. The technical monitor is Mr. Matthew L. Wilbur.

References

1. Cesnik, C. E. S. and Shin, S.-J., "On the Modeling of Integrally Actuated Helicopter Blades," *International Journal of Solids and Structures*, Vol. 38, No. 10-13, 2001, pp. 1765-1789.
2. Cesnik, C. E. S., Shin, S.-J., and Wilbur, M. L., "Dynamic Response of Active Twist Rotor Blades," *Smart Materials and Structures-Special Issue on Rotorcraft Applications*, Vol. 10, 2001, pp. 62-76.
3. Wilbur, M. L., Mirick, P. H., Yeager, Jr. W. T., Langston, C. W., Cesnik, C. E. S., and Shin, S.-J., "Vibratory Loads Reduction Testing of the NASA/ARMY/MIT Active Twist Rotor," *Journal of the American Helicopter Society*, Vol. 47, No. 2, 2002, pp. 123-133.
4. Shin, S.-J., Cesnik, C. E. S., and Hall, S. R., "Closed-loop Control Test of the NASA/ARMY/MIT Active Twist Rotor for Vibration Reduction," In *Proceedings of the American Helicopter Society 59th Annual Forum*, Phoenix, Arizona, May 6-8 2003.
5. Cesnik, C. E. S., Shin, S.-J., Wilkie, W. K., Wilbur, M. L., and Mirick, P. H., "Modeling, Design, and Testing of the NASA/ARMY/MIT Active Twist Rotor Prototype Blade," In *Proceedings of the American Helicopter Society 55th Annual Forum*, Montreal, Canada, May 25-27 1999.
6. Cesnik, C. E. S., and Shin, S.-J., "On the Twist Performance of a Multiple-Cell Active Helicopter Blade", Smart Materials and Structures, Vol. 35, (1), 1997, pp. 6-16.
7. Cesnik, C. E. S., Palacios, R., and Park, R.S., "Active Piezocomposite Actuator Distribution in Wing Cross Sections," SPIE's 10th Annual International Symposium on Smart Structures and Materials, San Diego, California, March 26, 2003.
8. Friedmann, P. P., "Helicopter Vibration Reduction Using Structural Optimization with Aeroelastic/Multidisciplinary Constraints - A Survey," *Journal of Aircraft*, Vol. 28, No. 1, 1991, pp. 8-21.
9. Walsh, J. L., Young, K. C., Tarzanin, F. J., Hirsh, J. E., and Young, D. K., "Optimization Issues with Complex Rotorcraft Comprehensive Analysis," In *Proceedings of the AIAA/USAF/NASA/ISSMO 7th Symposium on Multidisciplinary Analysis and Optimization*, St. Louis, MO, September 2-4 1998, AIAA Paper No. 98-4889.
10. Celi, R., "Recent Applications of Design Optimization to Rotorcraft," *Journal of Aircraft*, Vol. 36, No. 1, 1999, pp. 176-189.
11. Coleman, T., Branch, M. A., and Grace, A., *Optimization Toolbox For Use with MATLAB*, The MathWorks, Inc., Natick, MA, 1999.
12. Cesnik, C. E. S. and Palacios, R., "Modeling Piezocomposite Actuators Embedded in Slender Structures," In *Proceedings of the AIAA/ASME/ASCE/AHS/ASC 44th Structures, Structural Dynamics and Materials Conference-Adaptive Structures Forum*, Norfolk, VA, April 7-10 2003, AIAA Paper No. 2003-1803.

13. Bauchau, O. A., “Computational Schemes for Flexible, Nonlinear Multi-Body Systems," *Multibody System Dynamics*, Vol. 2, 1998, pp. 169-225.
14. www.mathworks.com The MathWorks, Inc., Natick, MA, 2004.
15. Hafka, R. T. and Gurdal, Z., *Elements of structural Optimization*, Academic Publishers, 1992.
16. Fletcher, R. and Powell, M. J. D., A Rapidly Convergent Descent Method for Minimization, Computer Journal, Vol. 6, pp. 163-168, 1963.